nature energy

ARTICLES

PUBLISHED: 25 JULY 2016 | ARTICLE NUMBER: 16111 | DOI: 10.1038/NENERGY.2016.111

Anion-redox nanolithia cathodes for Li-ion batteries

Zhi Zhu[1,2], Akihiro Kushima[1,2], Zongyou Yin[1,2], Lu Qi[3]*, Khalil Amine[4], Jun Lu[4]* and Ju Li[1,2]*

The development of lithium–air batteries is plagued by a high potential gap (>1.2 V) between charge and discharge, and poor cyclability due to the drastic phase change of O_2 (gas) and O^{x-} (condensed phase) at the cathode during battery operations. Here we report a cathode consisting of nanoscale amorphous lithia (nanolithia) confined in a cobalt oxide, enabling charge/discharge between solid $Li_2O/Li_2O_2/LiO_2$ without any gas evolution. The cathode has a theoretical capacity of 1,341 Ah kg^{-1}, a mass density exceeding 2.2 g cm^{-3}, and a practical discharge capacity of 587 Ah kg^{-1} at 2.55 V versus Li/Li$^+$. It also displays stable cycling performance (only 1.8% loss after 130 cycles in lithium-matched full-cell tests against $Li_4Ti_5O_{12}$ anode), as well as a round-trip overpotential of only 0.24 V. Interestingly, the cathode is automatically protected from O_2 gas release and overcharging through the shuttling of self-generated radical species soluble in the carbonate electrolyte.

In consumer electronics, electric vehicles, and grid-scale energy storage, Li-ion batteries occupy large market shares. Most of the cathodes used in lithium ion batteries are lithium transition metal oxides, but these cathodes have a gravimetric capacity limitation because redox reactions of heavy-metal cations[1,2] (Co, Mn, Ni, Fe, and so on) are required. In recent years, Li–air batteries[3,4] based on the light-anion redox O_2 (gas)/O^{x-} (condensed phase) have attracted much attention. However, severe challenges remain before they can be widely used. First, most Li–air batteries have a voltage gap above 1.2 V between charge and discharge, even if catalysts are used[5,6]. Second, few electrolytes currently available are stable enough to be used with both O_2 gas and Li_xO compounds. Third, a special and expensive membrane is required to block CO_2 and H_2O from air.

Because gas evolution and phase change between O_2 (gas) and O^{x-} (condensed phase) are required at the cathode in Li–air batteries, the nucleation and growth of such phase changes with a 10^4-fold difference in specific volume entail a huge overpotential (η, the difference between practical and theoretical potential values) with $\eta_{\text{discharging}} > 0.1$ V in O_2 (gas) $\rightarrow O^{x-}$ (condensed phase), and $\eta_{\text{charging}} > 1.1$ V in O^{x-} (condensed phase) $\rightarrow O_2$ (gas)[5,6]. The alarmingly large η_{charging} indicates severe kinetic bottlenecks in gas-evolving solid products (for example, Li_2O and Li_2O_2) being dynamically dismantled during charging[7]. The serious overpotential loss of charge and discharge (>1.2 V; refs 5,6,8) causes severe energy efficiency and thermal management problems. Repeated phase changes with large overpotential also cause chemo-mechanical damage that limits cyclability.

Here we develop an oxygen anion-redox cathode that does not release/take O_2 (gas). We show the phase changes occur between condensed-matter phases only—that is, between Li_2O (condensed), Li_2O_2 (condensed) and LiO_2 (condensed), where the average oxygen valence state $\bar{Z}$ changes from $\bar{Z} = -2$ (the purely ionic O^{2-} in Li_2O crystal) to $\bar{Z}$ as small as -0.5 in covalent-ionically bonded LiO_2 solid. While LiO_2 is metastable as a bulk crystal at room temperature, it appears to be stabilized by interfacial wetting[9] with a substrate, which has been supported by transmission electron microscopy (TEM) with a diffraction pattern matching the *ab initio* calculated crystal structure. In surface science[10] and metal-organic chemistry[11], it is well known that the O_2 molecule can be adsorbed as peroxide O_2^{2-} ($Z = -1$), as superoxide O_2^- ($Z = -0.5$), or as a mixture thereof that covers the surface. We hypothesize that a sub-10-nm porous substrate could stabilize a significant amount of LiO_2 (condensed) as an interfacial wetting layer (Fig. 1a). Since no oxygen gas evolves, we are able to fabricate an all-condensed-matter cathode for a fully sealed battery.

Nanolithia anion-redox cathode without O_2 evolution

We prepared 33 wt% Co_3O_4 as a nanoporous substrate and filled it with 67 wt% Li_2O (designated as sample NC-67, where NC stands for the nanolithia composite). The solid nanoporous skeleton is stable as the cathode cycles between Li_2O(condensed) $\leftrightarrow$ Li_2O_2(condensed) $\leftrightarrow$ LiO_2(condensed), providing structural integrity while the increased transport pathways and catalytic activity[12] reduce the overpotential significantly (by a factor of five, from $\eta > 1.2$ V to $\eta \approx 0.24$ V). In principle, other nanoporous skeletons may also be used for the NC. At the relatively narrow voltage range of testing (2.0–3.0 V versus Li/Li$^+$), the Co ions in Co_3O_4 remains in the +2 and +3 oxidation states[13], although there could be changes in the bonding pattern at the nanolithia/Co_3O_4 interface. The detailed configurations of the oxygen $\bar{Z} = -0.5 \leftrightarrow -2$ state in the active wetting layer need to be studied atomistically[14], but this becomes practically useful only if the cathode can be cycled reversibly. By keeping oxygen above the lowest ionicity of $\bar{Z} = -0.5$, we hope to maintain it as condensed matter rather than as a gas ($Z = 0$).

The following reactions apply to the NC cathode:

$$Li_2O_2 + 2Li^+ + 2e^- = 2Li_2O \quad U_1{}^0 = 2.86\,\text{V} \tag{1}$$

$$LiO_2 + 3Li^+ + 3e^- = 2Li_2O \quad U_2{}^0 = 2.88\,\text{V} \tag{2}$$

The above thermodynamic voltages $U_1{}^0$ and $U_2{}^0$ are calculated from the bulk crystal formation energies[15–17], although nanoscale

[1]Department of Nuclear Science and Engineering, Massachusetts Institute of Technology, Cambridge, Massachusetts 02139, USA. [2]Department of Materials Science and Engineering, Massachusetts Institute of Technology, Cambridge, Massachusetts 02139, USA. [3]College of Chemistry and Molecular Engineering, Peking University, Beijing 100871, China. [4]Chemical Sciences and Engineering Division, Argonne National Laboratory, Argonne, Illinois 60439, USA. *e-mail: qilu@pku.edu.cn; junlu@anl.gov; liju@mit.edu

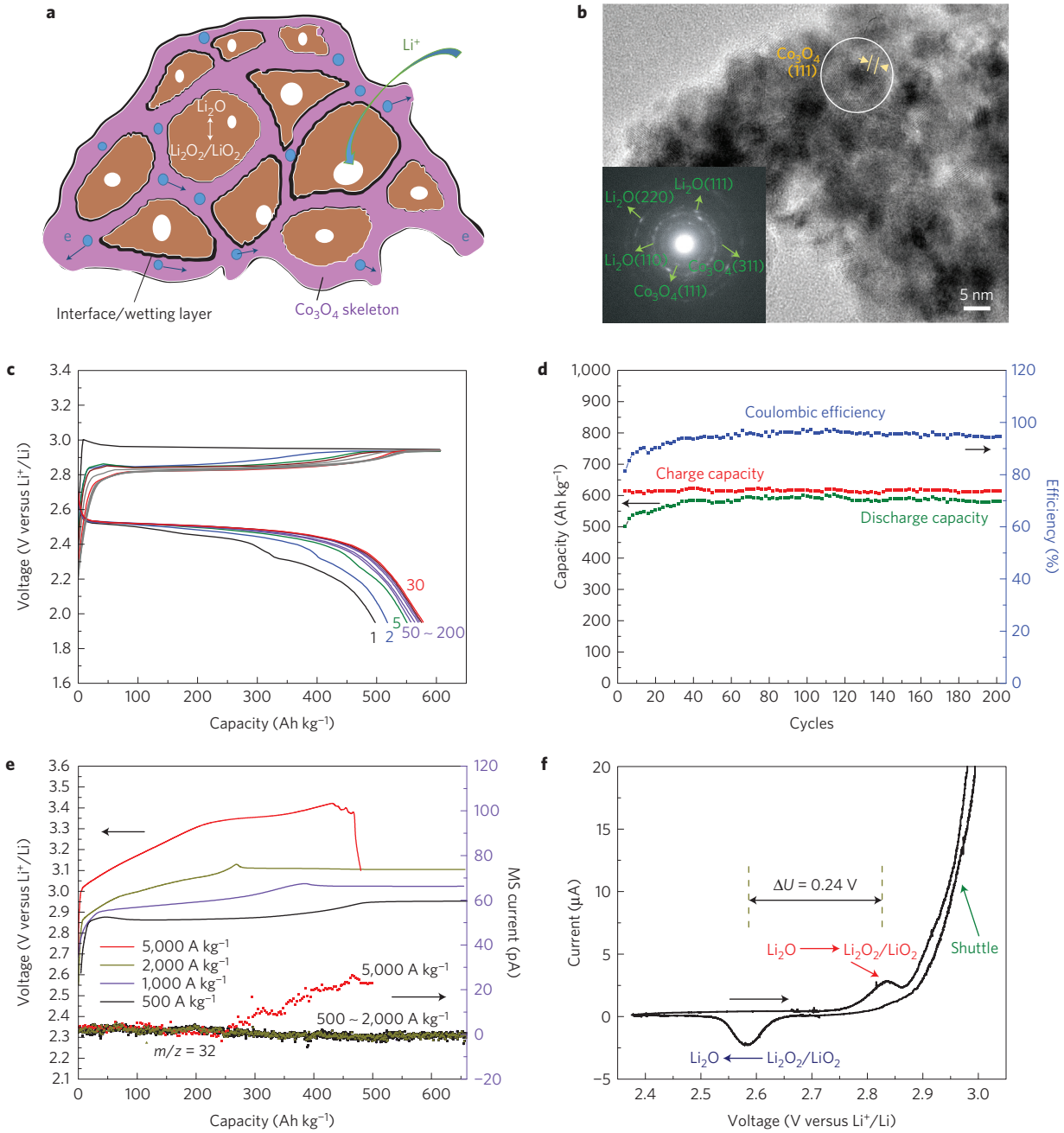

Figure 1 | The structure and electrochemical performance of nanolithia cathode. a, Schematic of Co_3O_4 skeleton wetted by amorphous $Li_2O/Li_2O_2/LiO_2$, the arrows indicate the diffusion paths of electrons and Li ions. **b**, Transmission electron microscopy (TEM) of the nanocomposite Li_2O and Co_3O_4 powder, the circled area is a representative structure of amorphous Li_2O confined within the Co_3O_4 skeleton. The inset is the selected-area electron diffraction pattern (SAED). **c**, Charge/discharge curves of NC-67 cathode in a coin-cell battery with Li metal anode. It was charged to 615 Ah kg^{-1} (based on Li_2O weight), then discharged to 2.0 V with constant current of 120 A kg^{-1} (based on Li_2O weight). Different cycles (1st–200th) are indicated with coloured lines. **d**, Cycling performance of charge/discharge capacity and Coulombic efficiency against Li metal anode under 120 A kg^{-1}. **e**, The charging curves (solid curves) and *in situ* differential electrochemical mass spectrometry (DEMS; dotted curves, for gas detection) at different current densities. **f**, Cyclic voltammogram of NC-67 between 2.35 and 3.0 V with a scan rate of 0.05 mV s^{-1}. The horizontal arrow indicates the scanning direction. The oxidation peak is related to the charge process from Li_2O to Li_2O_2/LiO_2, whereas the reduction peak is related to discharge from Li_2O_2/LiO_2 to Li_2O. The value of ΔU between the oxidation and reduction peaks is only 0.24 V. The high current above 2.9 V is attributed to shuttling species in electrolyte.

interfacial energy effects could shift and smear these voltages by tens of milli-electron volts. The theoretical capacity of Li_2O/LiO_2 is 1,341 Ah kg^{-1}, based on the weight of Li_2O. Although it is well known that bulk LiO_2 crystal is fairly unstable at room temperature, the LiO_2 (condensed) did form in our experiments due to the excellent catalysis and energetic stabilization by the nanoporous Co_3O_4 interfaces[9], akin to the superoxide O_2^- ($Z = -0.5$) adsorbate layer in surface science[10] and oxygen in haemoglobin proteins[11]. The NC cathode involves much higher capacity than the present cation-redox-based systems, even when the dead weight of Co_3O_4 is taken into account. As we will demonstrate below, lithium-matched full-cell batteries with low-cost ethylene carbonate/diethyl carbonate (EC/DEC) electrolyte can achieve gravimetric energy densities comparable to those of state-of-the-art Li–sulfur batteries[18], along

with higher voltage and very stable cycling, as well as with a 5× lower energy loss than the Li–air battery[7]. Okuoka *et al.*[19] proposed a similar redox reaction between Li_2O and Li_2O_2, and tested nanocomposite Li_2O with ball-milled Co_3O_4 as the cathode. Their preliminary results indicated the feasibility of using Li_2O/Li_2O_2 as the cathode. However, O_2 gas was inevitably generated when charging to above 190 Ah kg^{-1} around 3.2 V versus Li/Li^+ in that work. As it turns out in our work, a shuttling (some specific species dissolved in the electrolyte can carry electrons between cathode and anode through the electrolyte) mechanism[20] in the EC/DEC electrolyte can shunt the voltage automatically and indefinitely avoid the O_2 gas generation.

In contrast to the mechanical ball-milling approach of Okuoka *et al.*[19], we achieved much more intimate contact of Li_2O with sub-10 nm Co_3O_4 by using a highly scalable chemical synthesis method followed by calcination at 300 °C. Selected-area electron diffraction (SAED) in Fig. 1b and energy dispersive spectroscopy (EDS) in Supplementary Fig. 1 clearly indicate a mixture of Co_3O_4 and Li_2O, and most of the Li_2O nanoparticles are sphere-like (∼5 nm), and surrounded by a nanocrystalline Co_3O_4 skeleton. In this form, 'solid oxygen' in the condensed form (nanolithia) is no more than ∼3 nm away from a free surface or Co_3O_4 skeleton, and interfacial wetting effects are expected to significantly affect its electrochemical stability[9] and kinetics[21–23].

The charge/discharge and cycling performance of an NC-67 cathode (mass loading ∼2.0 mg cm^{-2}) opposite to a Li metal anode are shown in Fig. 1c,d and Supplementary Fig. 2. The NC-67 cathode has a discharge plateau of ∼2.55 V at a rate of 120 A kg^{-1} (based on Li_2O weight). The initial discharge capacity was 502 Ah kg^{-1} (based on Li_2O weight), then increased to 587 Ah kg^{-1} in a few cycles when charged to 615 Ah kg^{-1}. The discharge capacity loss was only 4.9% after 200 cycles. The charge plateau consists of two parts (Supplementary Fig. 2): part I, beginning at 2.80 V and gradually increasing to 2.91 V, can be due to $Li_2O \rightarrow Li_2O_2/LiO_2$, while part II, keeping nearly constant at ∼2.94 V, is due to a shuttling process in the electrolyte. *In situ* differential electrochemical mass spectrometry (DEMS, Supplementary Fig. 3a) showed no O_2 or CO_2 gas generation and the voltage never exceeded 2.95 V when charged at a constant current of 120 A kg^{-1}.

DEMS was also performed under different charging currents. As shown in Fig. 1e, the voltages of both the redox and shuttle plateaux increase with higher current. When charged at 500 A kg^{-1}, 1,000 A kg^{-1} and 2,000 A kg^{-1}, the shuttling produced the final shunting voltages of 2.96 V, 3.04 V and 3.14 V, respectively. The DEMS spectra indicates no O_2 generation, no matter how long the overcharging is. However, when charged at 5,000 A kg^{-1} (>10 C), the voltage continuously increases and O_2 gas evolves after the capacity reaches 250 Ah kg^{-1}, when the voltage is ∼3.4 V. The shuttling thus fails to suppress the voltage increase only when the shuttling species in the liquid electrolyte cannot support an extremely high current inside the cell (for example, 5,000 A kg^{-1}).

Transformation of the nanolithia composite cathode

X-ray photoelectron spectroscopy (XPS) plots in Supplementary Fig. 4 show that the Co ions in Co_3O_4 are electrochemically inactive in the charging process. To characterize the cathode transformation during cycling, *in situ* Raman spectroscopy was performed (Fig. 2a). On the Raman curve, a new peak at 780 ∼ 800 cm^{-1} appears when the cathode is charged to 200 Ah kg^{-1}. The peak is fairly broad, but centred at ∼790 cm^{-1}, which is consistent with Li_2O_2 (ref. 24). When further charged to 400 Ah kg^{-1}, this 780 ∼ 800 cm^{-1} peak becomes higher, but remains almost unchanged when charged to >500 Ah kg^{-1}. A new Raman peak around 1,110 ∼ 1,140 cm^{-1} emerges at above 500 Ah kg^{-1}, becoming gradually stronger when further charged to 700 Ah kg^{-1}, and keeping stable thereafter. This peak is similar to the 1,123 cm^{-1} peak reported for the O_2^- anion[24,25] ($\bar{Z} = -0.5$). Since it is not very sharp, it is likely that some form of amorphous LiO_2 (condensed) is generated. During charge/discharge, the Raman peaks increase in height, but do not change much in position or width. When the cathode is finally discharged to 2.0 V, the intensity is very weak at 780 ∼ 800 cm^{-1} (Li_2O_2 (condensed)) and totally disappears at 1,110 ∼ 1,140 cm^{-1} (LiO_2 (condensed)). The Raman spectra of the thoroughly washed cathode at different states of charge (SOCs) still show similar peaks at ∼790 cm^{-1} and ∼1,130 cm^{-1} (Supplementary Fig. 5). This result further confirms that the peroxide and superoxide species exist in the confined amorphous solid[21–23], instead of only solvated in the liquid electrolyte.

As shown in Fig. 1f, there is only one pair of broad redox peaks in the cyclic voltammogram (CV) for NC-67, suggesting a nanoscale mixture of $Li_2O/Li_2O_2/LiO_2$ (condensed) with smeared transition potentials. It is known that nanoparticles, especially with sub-10-nm diameter, have a shifted thermodynamic transition (such as shifted melting point) as well as a smeared order-parameter change[26] that is no longer infinitely sharp, as in the first-order phase transition of an infinite crystal. The most intriguing result is that the potential gap ($\Delta U = \eta_{charging} + \eta_{discharging}$) between the oxidation (2.82 V) and reduction (2.58 V) peaks (charge/discharge) is only 0.24 V. This gap is only one-fifth of that for the Li–air battery, indicating facile redox kinetics of the nanolithia. Specifically, the oxidation peak related to the charge plateau is 2.82 V, significantly lower than that reported for the Li–O_2 battery (usually >4.0 V). Such a small overpotential would vastly improve the usable energy efficiency in the battery and the severe heating issue.

ΔU in cycling is mainly caused by the energy barriers involved in electron and ion transfers and phase transformations. There is a huge structural difference between gas and condensed phases; thus, any transformation of oxygen involving gas ↔ solid would entail larger ΔU[7] and slower kinetics, which is the case for the Li–air battery. From the present work, we conclude that condensed ↔ condensed transformations, without gas phase participation, can have lower ΔU because the atomistic environment (at least in terms of density) of oxygen does not change drastically. This is especially so with the facile kinetics at the interface with Co_3O_4 and near-surface wetting layers in this work[21–23].

The SAED curve in Fig. 2b after charge shows that some low-index planes of the crystalline motif (such as (002), (101), (103) and (110) of crystalline Li_2O_2, and (110), (020), (011), (120) and (111) of crystalline LiO_2; ref. 27) roughly match in the charged product, even though many high-index planes do not match. The SAED result indicates that NC-67 changes to an amorphous $Li_2O/Li_2O_2/LiO_2$ mixture after charge, and this amorphization of cathode nanoparticles such as $LiFePO_4$ is well known[28]. The *in situ* X-ray diffraction (XRD) result (Supplementary Fig. 6) also suggests that most of the nanolithia turn amorphous in ten cycles, similar to that of the lithium–sulfur cathode[18] and lithium–aluminium anode[29]. The amorphous ↔ amorphous transformation during cycling would also have more facile kinetics compared to crystal ↔ crystal transformations, resulting in a much lower ΔU in Fig. 1f.

We also performed ^6Li NMR on the post-dimethoxyethane (DME)-washed cathode at different SOCs (all referenced to 1 M LiCl solution). As shown in Fig. 2c, the reference Li_2O and Li_2O_2 crystals have a sharp peak at 2.90 ppm and 0.21 ppm, respectively. The discharged NC-67 cathode has a strong peak at 2.90 ppm and a tiny peak at ∼0.21 ppm, indicating that the major component at this state is Li_2O, with a small amount of Li_2O_2 because of incomplete lithiation in the previous cycles. When charged to 400 Ah kg^{-1}, an obvious 0.21 ppm peak emerged, indicating that a significant amount of Li_2O_2 formed. When further charged to >600 Ah kg^{-1}, the peak at 0.21 ppm became higher than that at 2.90 ppm, but interestingly, another peak at −2.74 ppm appeared, regarding which we can find no report in the literature. To clarify

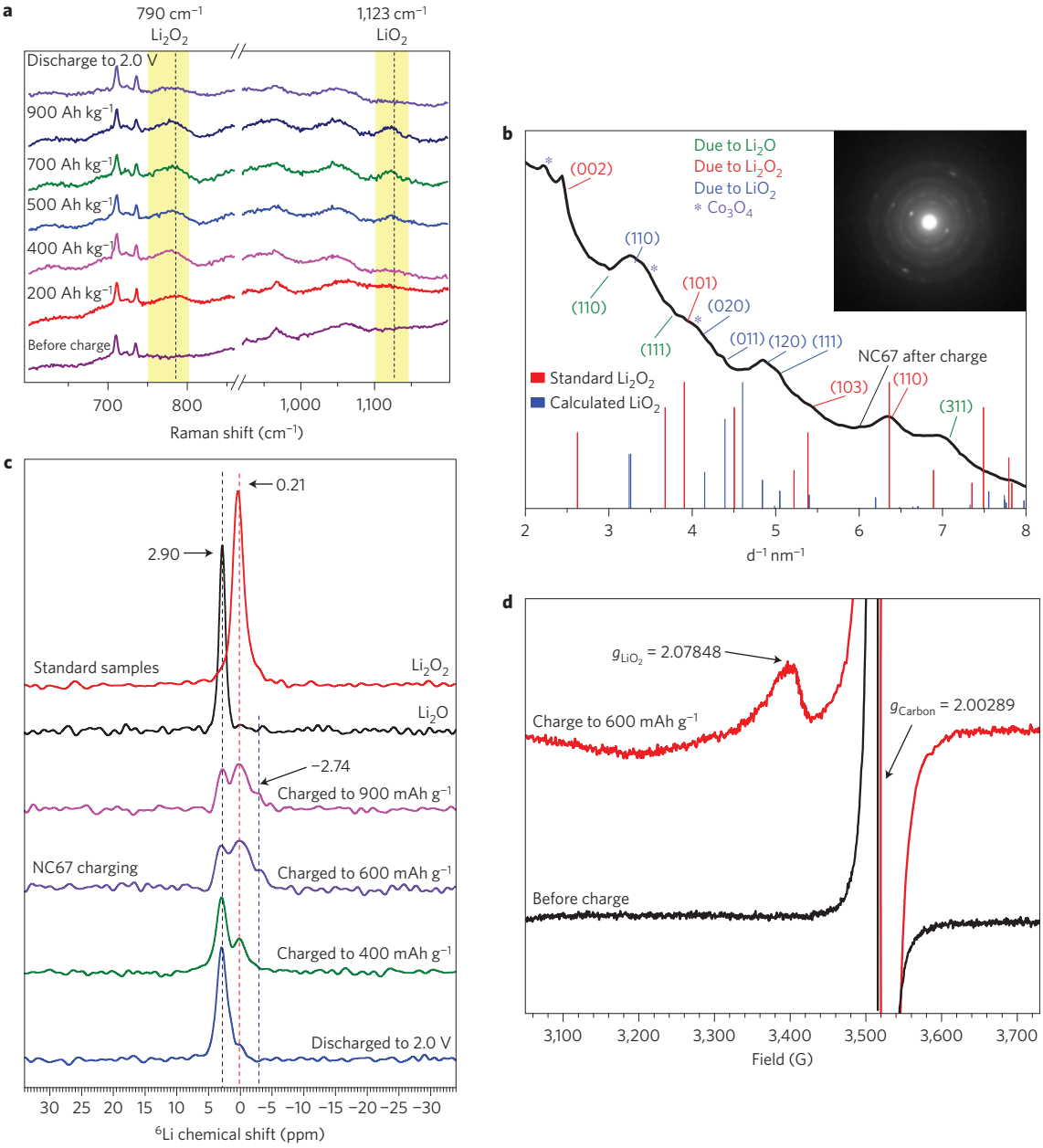

Figure 2 | The transformation of nanolithia during electrochemical cycling. a, *In situ* Raman at different charge/discharge states (the peaks in the yellow highlighted areas are due to Li_2O_2 and LiO_2, respectively). **b**, *In situ* SAED pattern of the charge product at 2.95 V. The curve was obtained by digital micrograph (Gatan) from the SAED pattern in the inset. **c**, ^{6}Li NMR of NC-67 at different charge/discharge states after DME washing, versus standard Li_2O and Li_2O_2 crystals, all referenced to 1 M LiCl solution in room temperature. **d**, Electron spin resonance (ESR) of the NC-67 cathode before and after charge at 70 K.

what this −2.74 ppm peak signifies, we calculated the chemical shift for different Li_xO crystals using density functional theory (DFT) (Supplementary Fig. 7). The calculated chemical shift for LiO_2 is −3.1 ppm versus Li_2O_2, or ∼−2.9 ppm versus the 1 M LiCl solution used in the experiment, matching very well with our experimental value of −2.74 ppm. Thus, our NMR measurement together with the DFT calculation firmly support the presence of LiO_2 in our deeply charged NC-67 electrode, proving the existence of an amorphous $Li_2O/Li_2O_2/LiO_2$ mixture stabilized by interfacial wetting.

Figure 2d shows the electron spin resonance (ESR) spectra for the NC-67 cathode at 70 K, before and after charge. It shows only an electron spin signal (g = 2.00289) from carbon before charge, indicating no other elements containing a single electron. However, another peak with g = 2.07848 appears after charging. This peak is due to the single-electron spin of the superoxide (O_2^-)[3]. The measured g-factor is between the *ab initio* calculated values for orthorhombic bulk LiO_2 (g = 2.085) and molecular LiO_2 (g = 2.045) (ref. 3), and is closer to the former, which is consistent with the structural motif of the nanoscale amorphous LiO_2 component.

Shuttling inside electrolyte

As stated previously, an automatic shuttling mechanism protects our cathode from overcharging and oxygen gas evolution only if the charge current $\leq$2,000 A kg^{-1}. To test its endurance, we performed galvanostatic charging at 120 A kg^{-1} for 72 h, and the voltage never exceeded 2.95 V (Fig. 3a). Upon the first discharge, the discharge

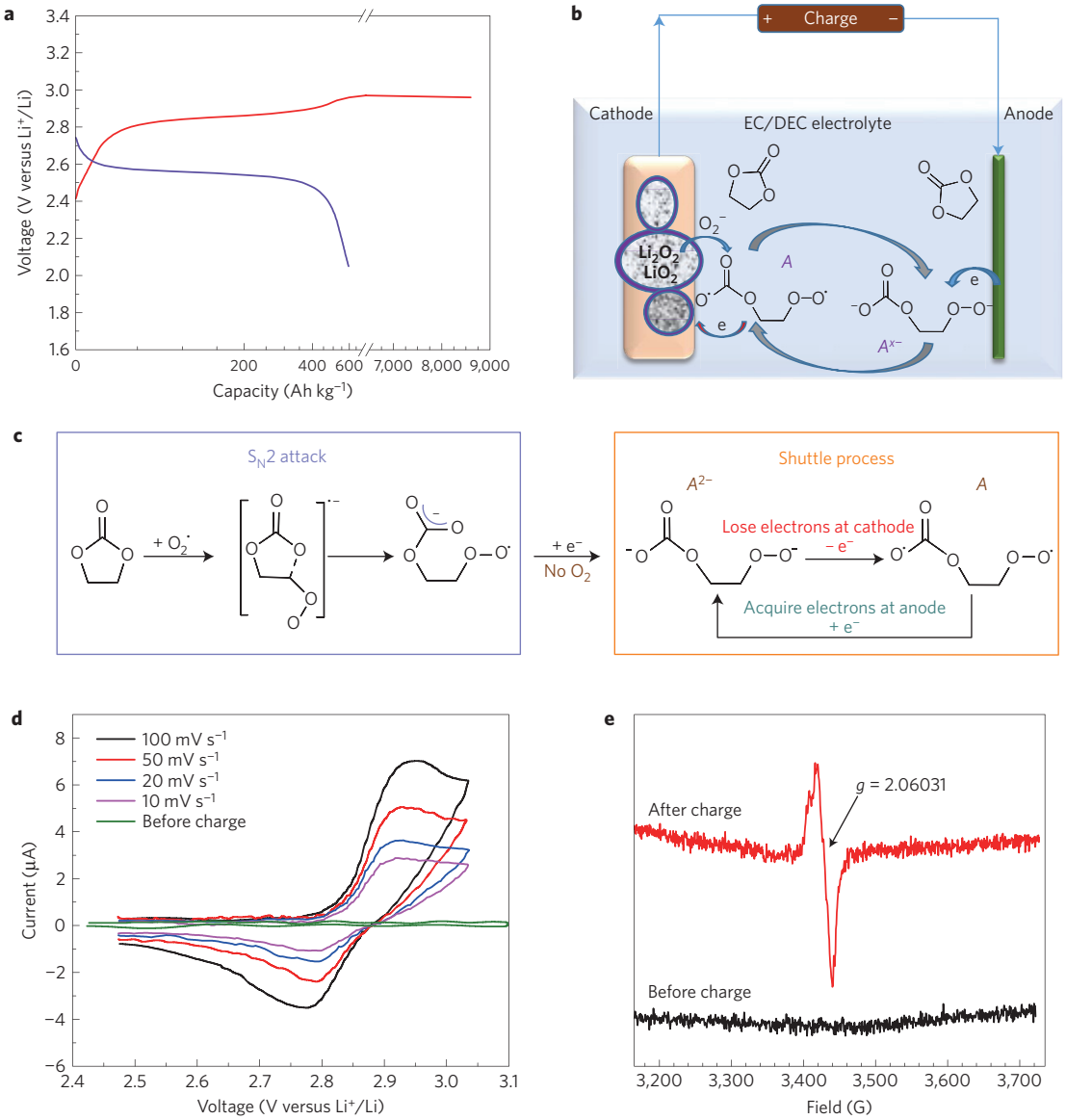

Figure 3 | Battery overcharge protection by electrolyte shuttling. a, Voltage profile of NC-67 cathode in three-day continuous charging to about 9,000 Ah kg^{-1}. **b**,**c**, Proposed reactions for the shuttling process at the end of charge. For EC in the electrolyte, the solvated O_2^- reacts with it, forming an intermediate radical *A*, the radical then diffuses to the anode and acquires electrons to become A^{2-}, which diffuses back and imparts the electron; the A/A^{2-} redox cycle thus provides the shunting current through the liquid electrolyte. **d**, Cyclic voltammogram of the liquid electrolyte extracted from a battery cell before/after charging, at scanning rates from 10 to 100 mV s^{-1} between 2.4 V and ~3.1 V in a Pt/Li/Li three-electrode system. **e**, *In situ* ESR of the isolated electrolyte extracted before/after charge, at room temperature.

capacity did not change, indicating no damage to the battery. If there had been an irreversible side reaction or oxygen release, such normal functioning after three-day overcharging would be impossible.

This shunting of potential has never been observed in the Li–air battery, and can be understood as shuttling[20] of soluble A/A^{x-} species, as shown in Fig. 3b,c. Because the Co_3O_4 encapsulation was not complete, some $Li_2O/Li_2O_2/LiO_2$ (condensed) was exposed to the liquid electrolyte, and O_2^- could be solvated. It is known that O_2^- (solvated) can attack the methylene group of carbonate solvent via the so-called S_N2 mechanism[30] shown in Fig. 3c. With EC as the electrolyte solvent, O_2^- (solvated) can be added to the methylene group, resulting in the ring opening and forming an intermediate peroxide radical *A* in the electrolyte[31]. *A* may be further oxidatively decomposed to CO_2, H_2O and Li_2CO_3 in a high O_2 (gas) partial pressure condition. However, here, because there is no O_2 gas evolution, the superoxoradicals do not decompose (Supplementary Fig. 3b) and can diffuse to the anode and acquire electrons to become A^{x-}, which, in turn, can diffuse back to the cathode, providing the shunting current through the liquid electrolyte.

To investigate the shuttling species in isolation, we disassembled a fully charged cell and carefully collected the electrolyte by thoroughly washing the cathode foil, membrane, anode and internal cavity of the cell with EC/DEC (1:1 by volume). Then, we investigated the diluted and isolated electrolyte by CV at different scanning rates in a Pt/Li/Li three-electrode system. The CVs of both the original and the collected diluted electrolyte after charging are shown in Fig. 3d. The CV curves indicate that the fresh electrolyte has no redox peaks, consistent with the expectation that EC/DEC is electrochemically stable between 2.4 V and ~3.1 V. However, the CV of the charged electrolyte shows classical redox behaviour, with an oxidation peak of 2.91 ~ 2.95 V and a reduction peak of 2.76 ~ 2.79 V. In addition, the oxidization

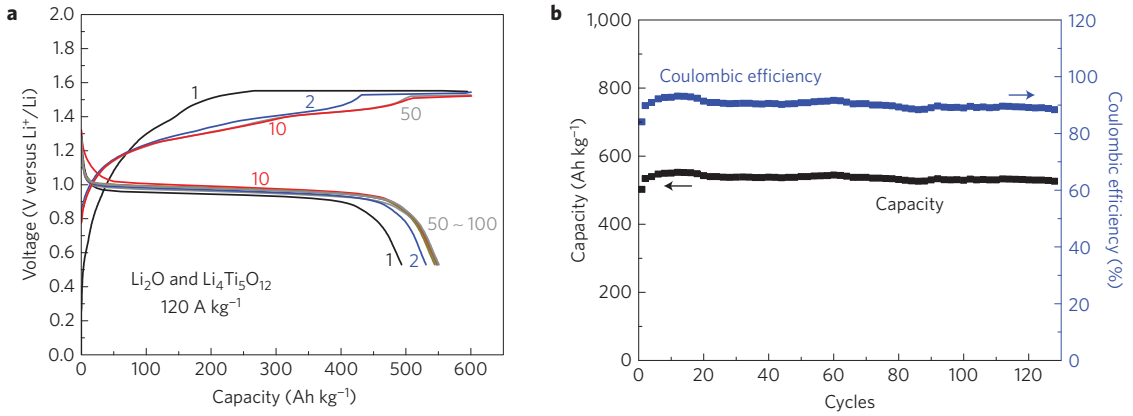

Figure 4 | Electrochemical performance of lithium-matched full-cell battery. a,**b**, Charge/discharge curves (**a**) and cycling performance (**b**) of NC-67 cathode versus $Li_4Ti_5O_{12}$ anode, whose Li capacity is only 110% that of the NC-67 cathode capacity. The coin cell was charged to 600 Ah kg^{-1} with a current of 120 A kg^{-1} based on Li_2O weight, then discharged to 0.5 V. This cell was fabricated with a Li-capacity ratio of 600:660 for NC-67 versus $Li_4Ti_5O_{12} \leftrightarrow Li_7Ti_5O_{12}$.

peak current (i_p) and the square root of the scanning rate ($v^{1/2}$) show a linear relationship ($R^2 = 0.9943$), indicating diffusion control, and further corroborating the existence of soluble redox couples in the electrolyte (Supplementary Fig. 8) that physically sustains the shuttling process.

In situ ESR was also performed to detect the shuttling species in the electrolyte at the end of charge, and the result is shown in Fig. 3e. The ESR result indicated no spin signal in the original, but an obvious radical signal at g = 2.06031 after charge. This g-factor is between the *ab initio* calculated values for orthorhombic bulk LiO_2 (g = 2.085) and molecular LiO_2 (g = 2.045) (ref. 3), but is closer to the latter. We thus infer that the organic superoxide radical coordinated with the solvent molecules acted as the shuttling species in the electrolyte at the end of charge, as illustrated in Fig. 3c.

Full-cell battery performance

To prove that our novel redox chemistry can drive a practical battery, we have assembled and tested a lithium-matched full cell using $Li_4Ti_5O_{12}$ (LTO) as the anode, with the Li capacity of $Li_4Ti_5O_{12} \leftrightarrow Li_7Ti_5O_{12}$ being only 110% that of the NC-67 cathode capacity (measured previously with a half-cell employing a superabundant amount of lithium metal). As shown Fig. 4a,b, although the NC-67/$Li_4Ti_5O_{12}$ full cell had a slightly lower capacity of 549 Ah kg^{-1} at a loading of 2 mg cm^{-2}, the full-cell capacity loss was only 1.8% after 130 cycles, so the cycling performance was even more stable than that versus the Li metal anode. This lithium-matched full-cell test indicates that even if a solid-electrolyte interphase (SEI) layer formed on the cathode surface, the SEI must be very stable during cycling[29], despite the necessarily large volume change of nanolithia $Li_2O/Li_2O_2/LiO_2$(all condensed).

Conclusions

We have exploited light-anion redox in a nanocomposite cathode with a sub-10-nm catalytic skeleton and amorphous nanolithia core. The gravimetric energy density is ~1,500 Wh kg^{-1} based on Li_2O weight, and 1,000 Wh kg^{-1} based on the weight of NC-67 composite (Co_3O_4+Li_2O). The mass density of our cathode paste (including binder and carbon black) exceeds 2.2 g cm^{-3}, making it also highly competitive in volumetric energy density against cathodes on the market. The NC cathode has a much reduced overpotential loss of only 0.24 V, as well as improved system-level weight and safety compared to Li–air batteries. Through the solvation and shuttling of A/A^{x-} in the electrolyte, O_2 gas generation is forestalled even if the battery is overcharged indefinitely, so this battery can work well in a completely sealed condition. Because Li_2O is in a lithiated state, the matching anode can be air-stable C, Al (ref. 29), Si (ref. 32), and so on. Additionally, the low-cost EC/DEC-based electrolyte solvent with $LiPF_6$ salt works very well.

Our nanocomposite still has much room for improvement, since complete encapsulation[29] (instead of partial encapsulation) may lead to an even larger Co_3O_4–lithia contact area, more efficient lithia utilization, and less O_2^- loss to the electrolyte (however, in such a scenario of complete encapsulation[29], to provide the shuttling, a new shuttling additive may need to be designed[20], at say 3.0 V versus Li/Li^+). In principle, sub-10-nm porous skeletons other than Co_3O_4 may also be adopted, such as nickel and manganese oxides. Besides a Li_2O core, one could also develop other light (and low-cost) anion-redox chemistries, for instance, redox couples involving ionic-covalent ClO_3^-, ClO^-, and so on in confined condensed-matter form without the generation of any gases (for example, Cl_2, O_2).

Methods

Preparation of nanocomposite Li_2O and Co_3O_4. We developed a one-pot chemical method to prepare nano-composite Li_2O and Co_3O_4 material. First, a mixture of Li_2O_2 (Sigma, 90%) and Li_2O (Aldrich, 99.5%) was added to $CoCl_2$ (Sigma, 99.5%) ethanol solution after ultrasonic treatment. The molar ratio of Li_2O_2:Li_2O:$CoCl_2$ is 1:n:1, where n dictates the Li_2O:Co_3O_4 weight percentage in the final fully oxidized product. After stirring for 2 h at room temperature, the obtained mixture was filtered and dried at 120 °C in vacuum. Then, the powder was sintered for 3 h at 300 °C in O_2 to derive the final product.

Material measurements. XRD measurements were carried out by means of a Bruker D8-Advance diffractometer using Cu Kα radiation, at 100 mA and 40 kV. The sample was scanned from 10° to 90° at a speed of 4° min^{-1}. The TEM images were taken on a JEOL JEM-2010 transmission electron microscope operating at 200 kV. The electronic valence structure of the samples was investigated through XPS. The prepared nano-composite cobalt oxide and lithia powder after the first charge and discharge were used for XPS characterization. The Raman spectra were measured using a Horiba Jobin-Yvon HR800 Raman spectrometer with a 633 nm laser. A 600 MHz Bruker NMR solid spectrometer was used to obtain ^{6}Li NMR with a main magnetic field of 14.1 T and a ^{6}Li Larmor frequency of 88.34 MHz. The rotors containing the samples were spun at a rate of ~10 kHz at room temperature to acquire the NMR spectra. All the chemical shifts obtained in the experiment were referenced to 1 M LiCl solution. A Bruker EMX ESR spectrometer with an ER 4199HS cavity and a Gunn diode microwave source producing X-band (9.859 GHz, ≈0.2 mW) radiation was used to detect the charged material and electrolyte. The magnetic field modulation was 100 kHz and the modulation amplitude was 1 G. The scan rates were 0.5 G s^{-1} with a time constant of 0.2 s.

***In situ* transmission electron microscopy (TEM).** A Nanofactory scanning tunnelling microscopy (STM)-TEM holder was used in the experiment. The holder is equipped with three-dimensional piezo-manipulator and biasing capability. The NC-67 cathodes were attached on a tungsten probe using conducting epoxy (Chemtronics CW2400) and mounted on one side of the holder. On the other side, we mounted another tungsten rod after scratching Li

metal to transfer a small piece of Li on the tip. The NC-67 and a piece of Li metal were brought into contact inside the TEM. By applying voltage on the working electrode versus the counter electrode (Li), Li^+ ions diffuse through the oxide layer. To drive the Li^+ out from NC-67, 2.95 V was applied to the working electrode with respect to the Li metal. The experiment was performed using a JEOL 2010F TEM operating at 200 kV. The SAED pattern was obtained after 30 min under 2.95 V.

Electrochemical tests. R2032 coin cells were used for the electrochemical tests in this work. Half-cells were fabricated from a cathode of 80 wt% NC-67 powder (that is, 67 wt% Li_2O, 33 wt% Co_3O_4), 15 wt% carbon black for electron conduction, and 5 wt% polyvinylidene fluoride (PVDF) binder, which was pasted on an Al current collector, at a loading of 2 mg cm^{-2}; an anode of Li metal sheets; a separator of Celgard 2400 polymer; and a commercial electrolyte. For the full cell, $Li_4Ti_5O_{12}$ was used as the anode, with 15 wt% C65 conductor and 5 wt% PVDF. The electrolyte solution was 1 M $LiPF_6$ dissolved in a mixture of EC and DEC with a volume ratio of 1:1, and 2 wt% vinylene carbonate additive. A LAND CT2001A 8-channel automatic battery test system (Wuhan Lanhe Electronics) was used for charging/discharging of the cells. An electrochemical workstation (Gamry Instr, Reference 3000) was used for the CV scanning.

A self-made quantitative DEMS was used to detect and analyse the gas during the cell testing. Two glued polyether ether ketone (PEEK) capillary tubes were used to inlet and outlet gas. The cell was fabricated in a glove box where O_2 <0.1 ppm. Then, the output tube was connected to a commercial Thermo mass spectrometer (MS). A high-purity Ar gas was used as the carrier gas with a flow rate of 3 ml min^{-1} during the cycling process. In the constant current charge/discharge process, charge/discharge currents were 100 mA g^{-1}, and MS spectra were collected every 1 min. In the cyclic voltammetry process, the scan rate was 0.05 mV s^{-1}, and MS spectra were collected every 20 s.

Received 9 December 2015; accepted 23 June 2016; published 25 July 2016

References

1. Zhu, Z. *et al.* Precise preparation of high performance spherical hierarchical $LiNi_{0.5}Mn_{1.5}O_4$ for 5 V lithium ion secondary batteries. *J. Mater. Chem. A* **1**, 5492–5496 (2013).
2. Zhu, Z. *et al.* Preparation of 4.7 V cathode material $LiNi_{0.5}Mn_{1.5}O_4$ by an oxalic acid-pretreated solid-state method for lithium-ion secondary battery. *J. Power Sources* **224**, 13–19 (2013).
3. Lu, J. *et al.* A lithium–oxygen battery based on lithium superoxide. *Nature* **529**, 377–382 (2016).
4. Lu, J. *et al.* Aprotic and aqueous $Li–O_2$ batteries. *Chem. Rev.* **114**, 5611–5640 (2014).
5. Débart, A., Paterson, A. J., Bao, J. & Bruce, P. G. α-MnO_2 nanowires: a catalyst for the O_2 electrode in rechargeable lithium batteries. *Angew. Chem.* **120**, 4597–4600 (2008).
6. Adams, B. D. *et al.* Current density dependence of peroxide formation in the $Li–O_2$ battery and its effect on charge. *Energy Environ. Sci.* **6**, 1772–1778 (2013).
7. Kushima, A. *et al.* Charging/discharging nanomorphology asymmetry and rate-dependent capacity degradation in Li–oxygen battery. *Nano Lett.* **15**, 8260–8265 (2015).
8. Lu, Y.-C. *et al.* Platinum-gold nanoparticles: a highly active bifunctional electrocatalyst for rechargeable lithium–air batteries. *J. Am. Chem. Soc.* **132**, 12170–12171 (2010).
9. Zhai, D. Y. *et al.* Interfacial effects on lithium superoxide disproportionation in $Li–O_2$ batteries. *Nano Lett.* **15**, 1041–1046 (2015).
10. Steininger, H., Lehwald, S. & Ibach, H. Adsorption of oxygen on Pt (111). *Surf. Sci.* **123**, 1–17 (1982).
11. Jones, R. D., Summerville, D. A. & Basolo, F. Synthetic oxygen carriers related to biological systems. *Chem. Rev.* **79**, 139–179 (1979).
12. Qi, L., Qian, X. & Li, J. Near neutrality of an oxygen molecule adsorbed on a Pt (111) surface. *Phys. Rev. Lett.* **101**, 146101 (2008).
13. Cabana, J., Monconduit, L., Larcher, D. & Palacin, M. R. Beyond intercalation-based Li-ion batteries: the state of the art and challenges of electrode materials reacting through conversion reactions. *Adv. Mater.* **22**, E170–E192 (2010).
14. Kang, S., Mo, Y., Ong, S. P. & Ceder, G. A facile mechanism for recharging Li_2O_2 in $Li–O_2$ batteries. *Chem. Mater.* **25**, 3328–3336 (2013).
15. Laoire, C. *et al.* Rechargeable lithium/TEGDME-$LiPF_6/O_2$ battery. *J. Electrochem. Soc.* **158**, A302–A308 (2011).
16. Laoire, C. O. *et al.* Influence of nonaqueous solvents on the electrochemistry of oxygen in the rechargeable lithium–air battery. *J. Phys. Chem. C* **114**, 9178–9186 (2010).
17. Lu, Y.-C. *et al.* The influence of catalysts on discharge and charge voltages of rechargeable Li–oxygen batteries. *Electrochem. Solid-State Lett.* **13**, A69–A72 (2010).
18. Wang, C. *et al.* Slurryless Li_2S/reduced graphene oxide cathode paper for high-performance lithium sulfur battery. *Nano Lett.* **15**, 1796–1802 (2015).
19. Okuoka, S.-i. *et al.* A new sealed lithium–peroxide battery with a co-doped Li_2O cathode in a superconcentrated lithium Bis(fluorosulfonyl)amide electrolyte. *Sci. Rep.* **4**, 5684 (2014).
20. Zhang, L., Zhang, Z.-C. & Amine, K. in *Lithium Ion Batteries - New Developments* (ed. Belharouak, I.) (InTech, 2012).
21. Yang, Z. H. *et al.* Glass transition dynamics and surface layer mobility in unentangled polystyrene films. *Science* **328**, 1676–1679 (2010).
22. Shin, K. *et al.* Enhanced mobility of confined polymers. *Nature Mater.* **6**, 961–965 (2007).
23. Ellison, C. J. & Torkelson, J. M. The distribution of glass-transition temperatures in nanoscopically confined glass formers. *Nature Mater.* **2**, 695–700 (2003).
24. Johnson, L. *et al.* The role of LiO_2 solubility in O_2 reduction in aprotic solvents and its consequences for $Li–O_2$ batteries. *Nature Chem.* **6**, 1091–1099 (2014).
25. Zhai, D. *et al.* Raman evidence for late stage disproportionation in a $Li–O_2$ Battery. *J. Phys. Chem. Lett.* **5**, 2705–2710 (2014).
26. Zhang, M. *et al.* Size-dependent melting point depression of nanostructures: nanocalorimetric measurements. *Phys. Rev. B* **62**, 10548–10557 (2000).
27. Lau, K. C., Curtiss, L. A. & Greeley, J. Density functional investigation of the thermodynamic stability of lithium oxide bulk crystalline structures as a function of oxygen pressure. *J. Phys. Chem. C* **115**, 23625–23633 (2011).
28. Kao, Y.-H. *et al.* Overpotential-dependent phase transformation pathways in lithium iron phosphate battery electrodes. *Chem. Mater.* **22**, 5845–5855 (2010).
29. Li, S. *et al.* High-rate aluminium yolk-shell nanoparticle anode for Li-ion battery with long cycle life and ultrahigh capacity. *Nature Commun.* **6**, 7872 (2015).
30. Bryantsev, V. S. & Blanco, M. Computational study of the mechanisms of superoxide-induced decomposition of organic carbonate-based electrolytes. *J. Phys. Chem. Lett.* **2**, 379–383 (2011).
31. Freunberger, S. A. *et al.* Reactions in the rechargeable lithium–O_2 battery with alkyl carbonate electrolytes. *J. Am. Chem. Soc.* **133**, 8040–8047 (2011).
32. Yang, Y. *et al.* New nanostructured Li_2S/silicon rechargeable battery with high specific energy. *Nano Lett.* **10**, 1486–1491 (2010).

Acknowledgements

We acknowledge financial support by NSF DMR-1410636. We thank Z. Wang for assistance with TEM measurements and analysis. We also thank H. Yao for help with the NMR data analysis and layout of the figures. This work was also partially supported by the US Department of Energy under Contract DE-AC0206CH11357 from the Vehicle Technologies Office, Department of Energy, Office of Energy Efficiency and Renewable Energy (EERE).

Author contributions

J.Li and Z.Z. conceived the original idea of this paper. Z.Z. performed the material synthesis and measurements, and then improved the experiments after discussions with J.Li and J.Lu. Z.Y. assisted with the Raman and XPS experiments; A.K. performed the TEM experiments and NMR calculation. Z.Z. and J.Li drafted the paper, and all authors revised it. L.Q. and K.A. provided many suggestions and guidance.

Additional information

Supplementary information is available online. Reprints and permissions information is available online at www.nature.com/reprints. Correspondence and requests for materials should be addressed to L.Q., J.Lu or J.Li.

Competing interests

The authors declare no competing financial interests.

PUBLISHED: 25 JULY 2016 | ARTICLE NUMBER: 16115 | DOI: 10.1038/NENERGY.2016.115

BATTERIES

Avoiding oxygen

In the development of lithium–air batteries, managing the phase change between gaseous oxygen and crystalline lithium peroxide is a key challenge. Now, a high-performing sealed battery with an oxygen anion-redox electrode is presented that does not involve any gas evolution.

Laurence J. Hardwick

Energy storage in the form of rechargeable batteries is becoming increasingly important for a range of applications including transportation and grid reserves. Recent interest in non-aqueous metal–oxygen batteries, particularly lithium–oxygen ($Li–O_2$), has stemmed from their high theoretical gravimetric energy densities[1]. In $Li–O_2$ batteries, the reactant (O_2) is not contained within the cell; instead, it enters from outside and undergoes reduction at the positive electrode, and is then combined with Li^+ to form lithium peroxide (Li_2O_2) during discharge. The product Li_2O_2 has a much lower molecular weight to electron ratio than typical intercalation compounds used in Li-ion batteries (that is, 23 for Li_2O_2 versus 98 for $LiCoO_2$), which is the reason why the theoretical energy density of $Li–O_2$ greatly surpasses that of Li-ion. The challenges, on the other hand, are related to mass transport, getting O_2 to the electrode surface so it can be reduced at sufficiently fast rates in order to have a useful power capability and preventing blockage of the electrode pores during the precipitation of solid Li_2O_2. In addition, the air stream will have to be virtually free of moisture and CO_2 to avoid deleterious side reactions. Writing in *Nature Energy*[2], Ju Li and colleagues from Massachusetts Institute of Technology, Peking University and Argonne National Laboratory now demonstrate a sealed lithium-ion cell, as opposed to the open system of $Li–O_2$ batteries, with an oxygen anion-redox ($O^{2-}/O_2^-/O_2^{2-}$) electrode, which avoids the uptake and release of O_2.

The key idea behind the work is the development of an intimately mixed matrix of nanoscale lithium oxide, also known as lithia (Li_2O), and cobalt oxide (Co_3O_4). Li_2O exists as evenly dispersed domains on the order of 5 nm within the Co_3O_4. When oxidized, Li_2O can be transformed to lithium superoxide (LiO_2) and Li_2O_2, via redox reactions between O^{2-}/O_2^-, O^{2-}/O_2^{2-}, and possibly O_2^{2-}/O_2^-. In particular, the researchers showed that the LiO_2 and Li_2O_2 can be reduced back to Li_2O with a discharge capacity of around 550 Ah kg^{-1}, and the cycle can be repeated over 100 times. When used as the positive electrode in a Li-ion cell, a specific energy of 1,000 Wh kg^{-1} was shown, which rivals the $Li–O_2$ cell and outcompetes the state-of-the-art Li-ion technology by a factor of 2.5–3 at the materials level[1]. The cell also showed a minor voltage gap of 0.24 V between discharge and charge, implying possible high roundtrip efficiencies in operation.

A fascinating aspect of the study is the internal generation of a stable redox shuttle, that is, a redox species that diffuses in-between both electrodes essentially allowing electrons to flow through the electrolyte. A redox shuttle in this example could be thought of as a 'chemical short circuit'. As shown in Fig. 1, the redox shuttle (Sh^-) is created from the reaction between surface exposed LiO_2 and the electrolyte solvent (ethylene carbonate). Sh^- diffuses to the negative electrode where it is further reduced (Sh^{2-}); subsequently the shuttle (Sh^{2-}) diffuses back to the positive electrode where it is oxidized. The redox

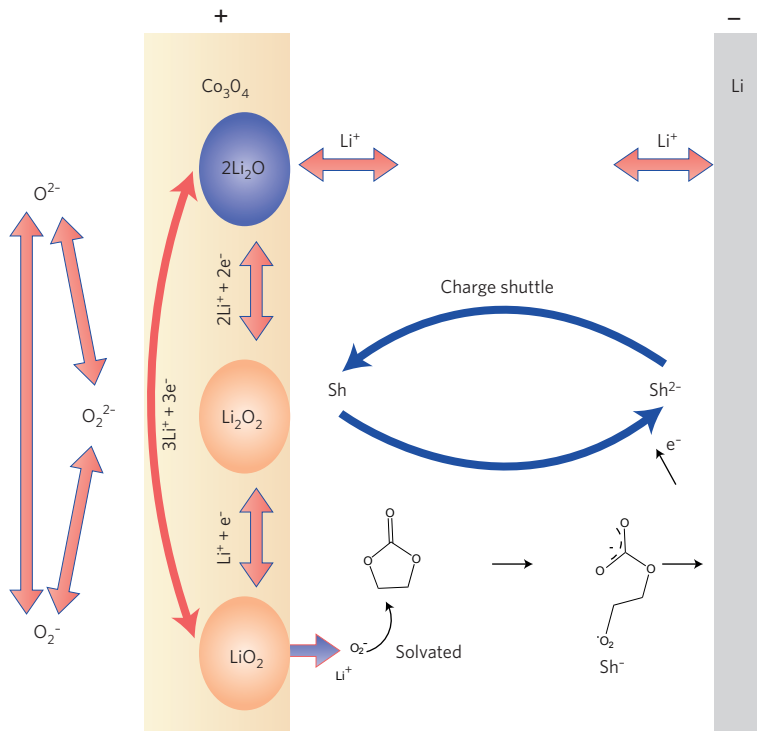

Figure 1 | Operation mechanism of the sealed Li-ion cell. A reversible lithium oxide–peroxy/superoxide positive electrode and lithium metal negative electrode are schematically shown. Nanoscale lithium oxide (Li_2O) within a Co_3O_4 matrix can be reversibly transformed to lithium peroxide (Li_2O_2) and lithium superoxide (LiO_2) at the positive electrode. The identity and transformation pathway of each redox active oxygen species is presented to the left of the Li-ion cell. Within the cell a redox shuttle (represented by 'Sh', 'Sh^-' and 'Sh^{2-}') is generated from the reaction of surface exposed LiO_2 and the solvent ethylene carbonate. The shuttle (Sh^-) diffuses to the negative electrode where it is further reduced (Sh^{2-}); subsequently the shuttle (Sh^{2-}) diffuses back to the positive electrode where it is oxidized by giving up two electrons (Sh). The shuttle process protects the cell from oxygen gas release during overcharge.

shuttle therefore allows the movement of current through the electrolyte, preventing potential O_2 evolution. Note that the redox shuttle maintains the electrode potential at 2.95 V vs Li^+/Li under a current load of 0.12 A g^{-1} (based on the mass of Li_2O). This is important because O_2 can only be thermodynamically liberated from Li_2O_2 above 2.96 V ($Li_2O_2 \rightarrow O_2 + 2Li^+ + 2e^-$). Indeed, the researchers monitored the gas release from the cell and did not detect O_2 during charging. Only when currents larger than 5 A g^{-1} were used to charge the cell, was the limit of the shuttle's ability to prevent the oxidation to O_2 reached. It is the ability of the redox shuttle to prevent O_2 evolution that significantly advances the system pioneered by Okuoka and co-workers[3]. In that work Li_2O was also shown to convert to Li_2O_2 during charge, but without an internal charge shuttle they could not prevent O_2 gas release beyond a capacity of around 200 Ah kg^{-1}.

The choice of electrolytes, it seems, is essential in the prevention of O_2 release. In their report Okuoka *et al.*[3] used a concentrated (4 molar) lithium bis(fluorosulfonyl)amide salt dissolved in acetonitrile, whilst Li and colleagues[2] adopted the organic carbonate based electrolyte (ethylene carbonate and diethylene carbonate with the salt lithium hexafluorophosphate) that is regularly used in Li-ion batteries. In oxygen-saturated organic carbonate electrolytes, any LiO_2 generated, will irreversibly react[4], forming a variety of soluble and insoluble side-reaction products, which was the scourge of early Li–O_2 battery work while more stable solvents were being sought[4,5]. However, as demonstrated by Li and colleagues[2], when the partial pressure of the O_2 is low, a superoxoradical species maintains its stability and acts as the redox shuttle between the positive and negative electrode preventing O_2 evolution during overcharge.

In order to confirm that Li_2O converts to both Li_2O_2 and LiO_2 during charge and returns back to Li_2O upon discharge, the research team also undertook Raman, ^{6}Li nuclear magnetic resonance, electron paramagnetic resonance spectroscopy measurements at various charge capacities and then at the full discharge capacity. The spectral information from these techniques provided strong evidence for the proposed chemical reactions. Nevertheless, the exact chemical structure of the shuttle species still requires further investigation. Going beyond this work it will be interesting to see whether an analogous sodium version of this system can be demonstrated. Moreover, an examination of redox shuttles that operate at about 3 V versus Li^+/Li in similar and alternative electrolytes could allow the prevention of O_2 evolution at even higher current rates.

Developments in Li-ion batteries based upon intercalation chemistry are approaching their theoretical energy storage limit[6]. Worldwide, numerous alternative battery chemistries are undergoing intense research to move beyond what Li-ion may offer in terms of energy storage. As yet, no obvious front runner has emerged. The work from Li and colleagues has added a further promising high energy storage battery system into the mix. Importantly the study includes a detailed spectroscopic understanding of the underlying (electro)chemical reactions involved that will greatly facilitate a rational basis towards future development of this system. ❐

Laurence J. Hardwick is at Stephenson Institute for Renewable Energy, Department of Chemistry, University of Liverpool, Liverpool L69 7ZF, UK.
e-mail: hardwick@liverpool.ac.uk

References

1. Bruce, P. G., Freunberger, S. A., Hardwick, L. J. & Tarascon, J. M. *Nature Mater.* **11,** 19–29 (2012).
2. Zhu, Z. *et al. Nature Energy* **1,** 16111 (2016).
3. Okuoka, S.-I. *et al. Sci. Rep.* **4,** 5684 (2014).
4. Vivek, J. P., Berry, N., Papageorgiou, G., Nichols, R. J. & Hardwick, L. J. *J. Am. Chem. Soc.* **138,** 3745–3751 (2016).
5. Freunberger, S. A. *et al. J. Am. Chem. Soc.* **133,** 8040–8047 (2011).
6. Van Noorden, R. *Nature* **507,** 26–28 (2014).

nature energy

SUPPLEMENTARY INFORMATION

ARTICLE NUMBER: 16111 | DOI: 10.1038/NENERGY.2016.111

Anion-redox nanolithia cathodes for Li-ion batteries

Zhi Zhu[1,2], Akihiro Kushima[1,2], Zongyou Yin[1,2], Lu Qi[3]*, Khalil Amine[4], Jun Lu[4]*

and Ju Li[1,2]*

[1]Department of Nuclear Science and Engineering, Massachusetts Institute of Technology, Cambridge, Massachusetts 02139, USA.

[2]Department of Materials Science and Engineering, Massachusetts Institute of Technology, Cambridge, Massachusetts 02139, USA.

[3]College of Chemistry and Molecular Engineering, Peking University, Beijing 100871, China.

[4]Chemical Sciences and Engineering Division, Argonne National Laboratory, Argonne, Illinois 60439, USA.

DOI: 10.1038/NENERGY.2016.111

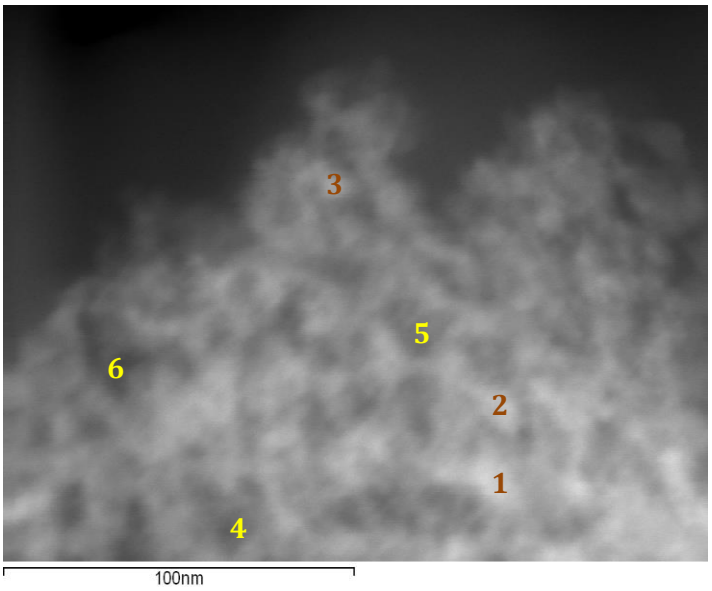

	Sites	Co:O
Cores	1	**1:6.61**
	2	**1:5.32**
	3	**1:4.79**
Skeleton	4	**1: 2.08**
	5	**1:1.86**
	6	**1:1.47**

Supplementary Fig. 1: EDS image of the NC material, and the ratios of Co:O at various locations marked in the image

We have tried to get the atom ratio in various core and skeleton locations to get the Co and O atoms distribution, shown in Fig 1. We can clearly see that the ratios of Co: O in core locations (bright field in EDS image) were between 1: 6.61 and 1: 4.79, but those of skeleton locations were about 1: 2.08~1: 1.47, close to that of Co_3O_4. Thus, we can infer that the skeleton is mainly Co_3O_4, while the cores are mainly Li_2O.

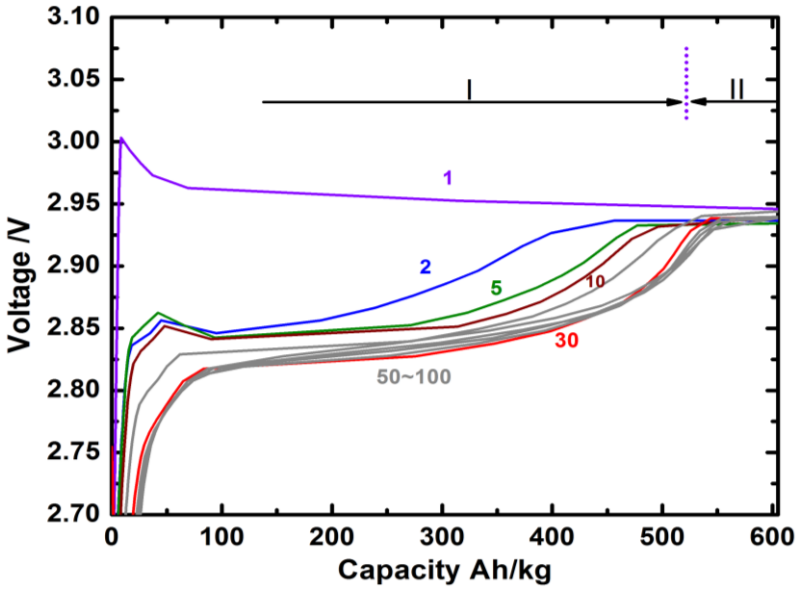

Supplementary Fig. 2: Magnified view of charging curves at 120 A/kg

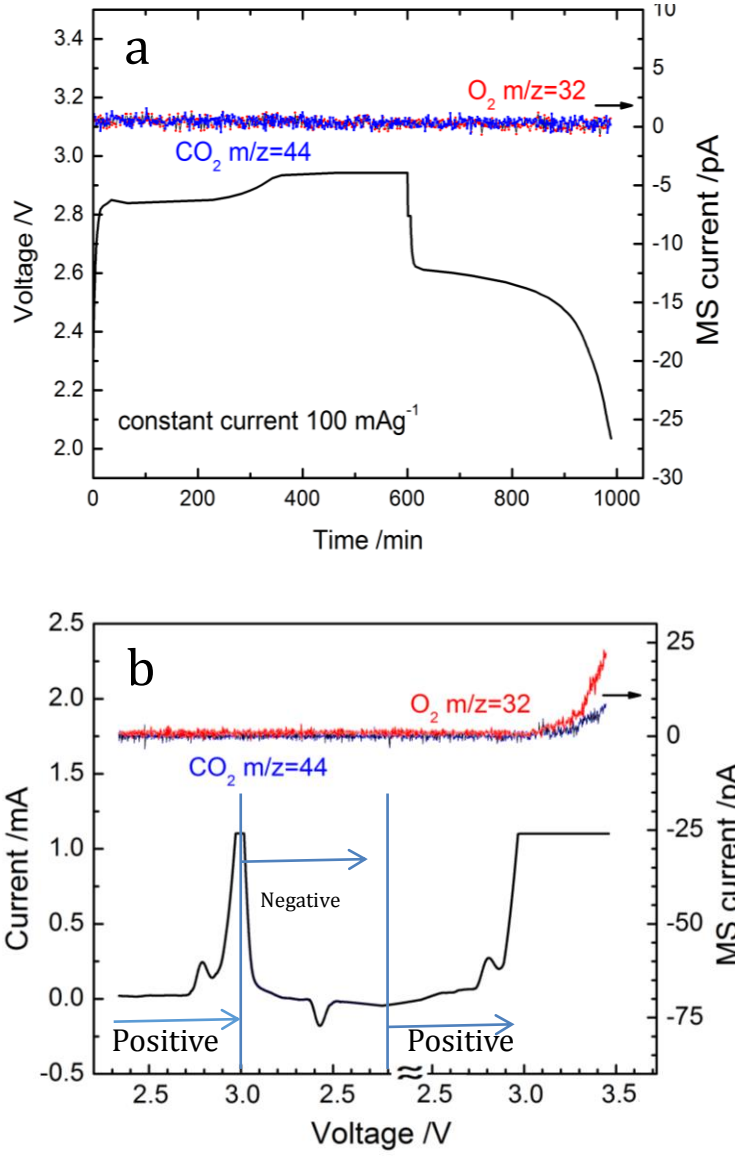

Supplementary Fig. 3: DEMS of NC-67 with (**a**) constant current test in a charge and immediately discharge process; (**b**) cyclic voltammetry, the first two segments are tested between 2.2V~3.0 V, and the third cycle is up to 3.5 V

We had DEMS tests with both constant current charging/discharging (*m/z*=32 for O_2 and *m/z*=44 for CO_2) and cyclic voltammetry. Both results are shown in Fig 3. In Fig 3a, we can clearly see that there is no O_2 and CO_2 gas generated (in the whole process, though it was overcharged for another 200 min (shuttle may occur from around 600 $mAhg^{-1}$ to 1000 $mAhg^{-1}$). Under CV, the battery was first positive scanning to 3.0 V, then negative scanning to 2.2 V, then positive scanning again to about 3.5 V. In Fig 3b, there are no O_2 and CO_2 gas generated in the initial two CV segments, as the voltage range is between 2.2 V-3.0 V, though the current above 2.90 V is very high and exceeds the upper limit of measurement near 3.0 V. However, when enforcing a large enough current to increase the voltage to >3.11 V, O_2 gas was detected and the rate for O_2 generation in MS is increasing. And nearly at the same time after the O_2 generation, CO_2 was also detected above ~3.12V. This result is

DOI: 10.1038/NENERGY.2016.111

consistent with the predication that the irreversible decomposition of EC electrolyte to CO_2 would occur *only after* the presence of O_2 ($\bar{Z}$=0), but would stay as reversible superoxide radical in the O_2-free condition, resulting in a shuttle process.

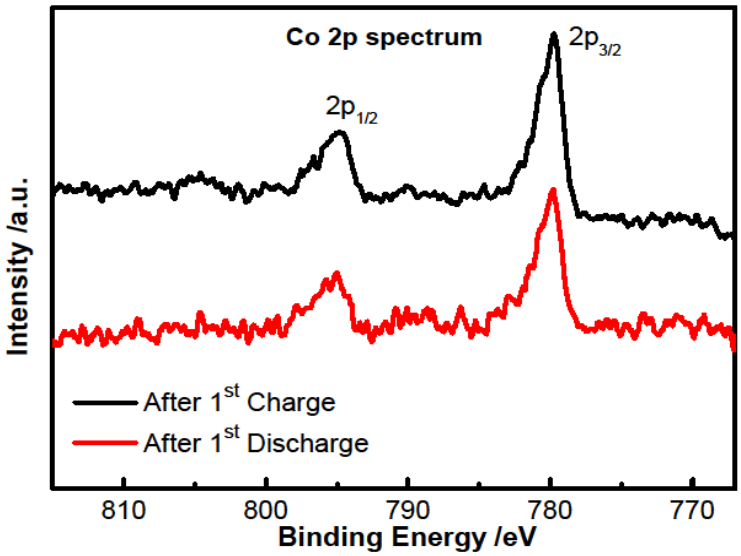

Supplementary Fig. 4: XPS after the first charge and discharge, indicating unchanged valence of Co

X-ray photoelectron spectroscopy (XPS) plots after the first charge and discharge are presented in Fig 4. The two peaks at ~795 eV (Co $2p_{1/2}$) and ~780 eV (Co $2p_{3/2}$) reveal that the composition of cobalt oxide is Co_3O_4. The peak positions of Co $2p_{1/2, 3/2}$ never change during electrochemical cycling, thus Co ions supply negligible redox reactions for the electrochemical activity. This finding also agrees with the notion that at the voltage range of testing (2-3 V *vs* Li/Li^+), the Co ions in Co_3O_4 are electrochemically inactive and should remain in the +2 and +3 oxidation state (note that Co_3O_4 has been widely used as an anode, but the active voltage range is below 1.2 V *vs* $Li/Li^{+2,+3}$).

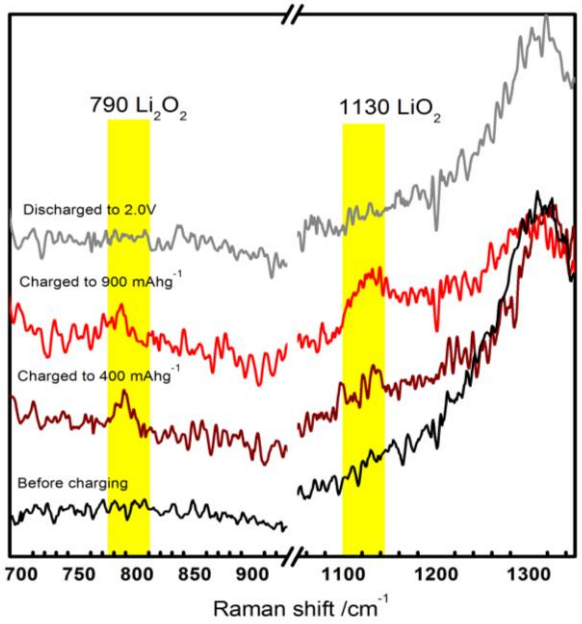

Supplementary Fig. 5: Raman curve of NC-67 at different states of charge/discharge (SOCs/SODs), all the curves are obtained after thorough washing by dimethoxyethane (DME) very quickly

Because superoxide O_2^- ($\bar{Z}$= -0.5) species can exist either as confined amorphous solid or solvated in the liquid electrolyte, we opened the cell at different SOCs/SODs, thoroughly washed the cathode with DME to remove the original electrolyte and solvated ions. Then the cathode foil was tested with Raman and the results were shown in Fig 5. Though the noise increased, the peaks were still at ~790 cm^{-1} and ~1130cm^{-1}, with a FWHM of 20 cm^{-1} and 30 cm^{-1}, respectively.

DOI: 10.1038/NENERGY.2016.111

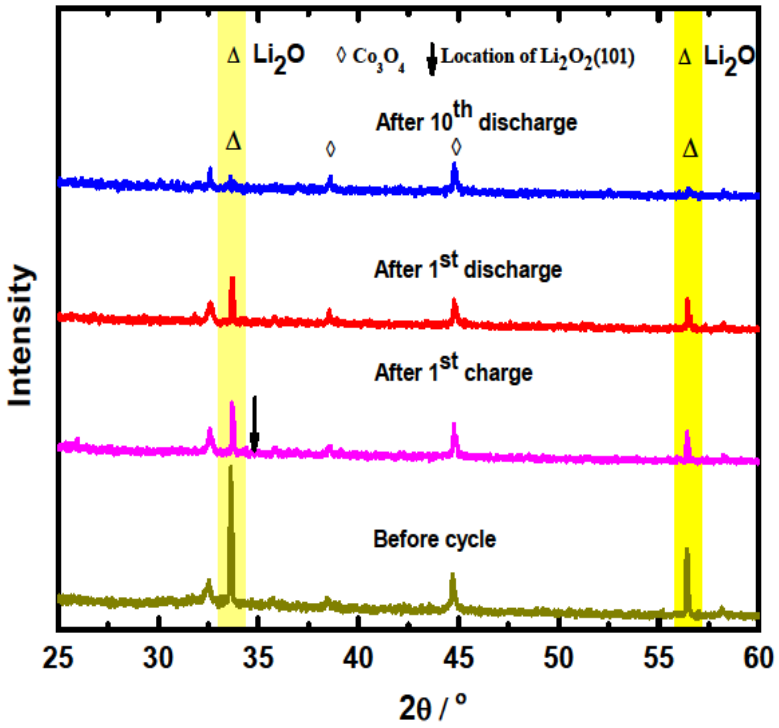

Supplementary Fig. 6: *In situ* XRD (on electrode foil) at different SOCs/SODs (the peaks in yellow highlighted area are due to Li_2O);

Fig 6 shows the XRD curves of the cathode at different SOCs/SODs and cycles. The original peaks of the Li_2O crystal decreased significantly in the first charge process, did not recover in the following discharge process, and almost disappeared after 10 cycles.

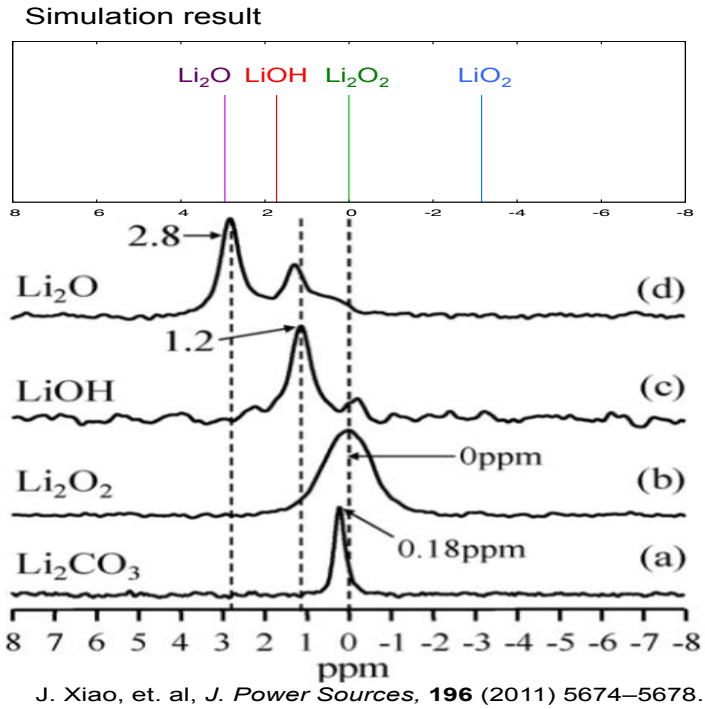

J. Xiao, et. al, *J. Power Sources*, **196** (2011) 5674–5678.

Supplementary Fig. 7: Calculated ^{6}Li NMR chemical shifts for Li_2O, LiOH, Li_2O_2, and LiO_2 in comparison with NMR spectra reported in *J. Power Sources*, **196** (2011) 5674

To identify the NMR peaks observed in the experiment, we calculated chemical shifts for different Li-O systems by DFT simulation. The chemical shifts were calculated using Vienna Ab Initio Simulation Package (VASP) with planewave basis[1,2] and projected-augmented wave (PAW) potentials.[3,4] Exchange-correlation functionals used in the calculation was in a Perdew–Berke–Ernzerhof (PBE)[5] form within the generalized-gradient approximation (GGA).[6]

The simulation cells for Li_2O, Li_2O_2, and LiO_2 consisted of 8 Li and 4 O atoms, 4 Li and 4 Li atoms, and 2 Li and 4 O atoms, respectively. The structure of LiO_2 reported in ref. 7 was used in the calculation. After the cell parameters and the atom positions were optimized by conjugate gradient energy minimization, the chemical shifts were calculated using the linear response method.[8,9] The calculated chemical shift values were shifted to match the experimentally obtained NMR chemical shift value of Li_2O_2. An energy cutoff of 450 eV was used for the structural optimization and 580 eV was used for the chemical shift calculation. Monkhorst–Pack **k**-point sampling[10] of $5 \times 5 \times 5$, $8 \times 8 \times 4$, and $6 \times 6 \times 3$ were selected for Li_2O, Li_2O_2, and LiO_2, respectively.

Fig 7 shows the calculated chemical shifts in comparison with the experiments. The calculated values are shifted to match the experimental NMR peak of Li_2O_2. The simulation results were benchmarked to an experimental data reported in *J. Power Sources*, **196** (2011) 5674 by J. Xiao. The calculated chemical shifts for Li_2O, LiOH, and Li_2O_2 matches well with the literature. The simulated value for LiO_2 appears on the negative side and easily distinguished from the others. We cannot find literature report for LiO_2 chemical shift either by calculation or by experiment.

The obtained new peak in our NMR experiment matches our calculated chemical shift value of LiO_2. The NMR measurement together with DFT modeling provides additional support for the presence of LiO_2 in our deeply discharged NC electrode.

DOI: 10.1038/NENERGY.2016.111

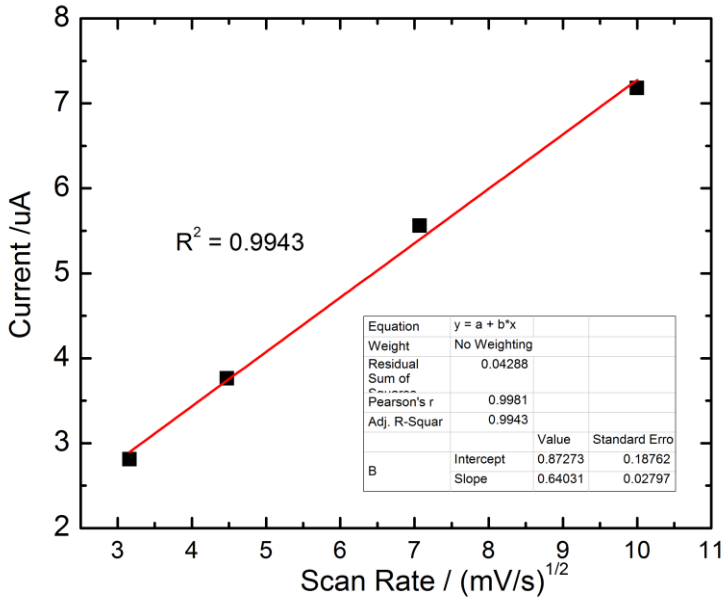

Supplementary Fig. 8: The relationship between current peak i_p and square root of scanning rate $v^{1/2}$ in CV measurement

Supplementary References

(1) Kresse, G.; Hafner, J. Ab Initio Molecular Dynamics for Liquid Metals. *Phys. Rev. B* **1993**, *47*, 558.

(2) Kresse, G.; Furthmller, J. Efficient Iterative Schemes for Ab Initio Total-Energy Calculations Using a Plane-Wave Basis Set. *Phys. Rev. B* **1996**, *54*, 11169.

(3) Blchl, P. E. Projector Augmented-Wave Method. *Phys. Rev. B* **1994**, *50*, 17953.

(4) Kresse, G.; Joubert, D. From Ultrasoft Pseudopotentials to the Projector Augmented-Wave Method. *Phys. Rev. B* **1999**, *59*, 1758.

(5) Perdew, J. P.; Burke, K.; Ernzerhof, M. Generalized Gradient Approximation Made Simple. *Phys. Rev. Lett.* **1996**, *77*, 3865.

(6) Perdew, J. P.; Chevary, J. A.; Vosko, S. H.; Jackson, K. A.; Pederson, M. R.; Singh, D. J.; Fiolhais, C. Atoms, Molecules, Solids, and Surfaces: Applications of the Generalized Gradient Approximation for Exchange and Correlation. *Phys. Rev. B* **1992**, *46*, 6671.

(7) Das, U.; Lau, K. C.; Redfern, P. C.; Curtiss, L. A. Structure and Stability of Lithium Superoxide Clusters and Relevance to Li–O2 Batteries. *J. Phys. Chem. Lett.* **2014**, *5*, 813–819.

(8) Pickard, C. J.; Mauri, F. All-Electron Magnetic Response with Pseudopotentials: NMR Chemical Shifts. *Phys. Rev. B* **2001**, *63*, 245101.

(9) Yates, J. R.; Pickard, C. J.; Mauri, F. Calculation of NMR Chemical Shifts for Extended Systems Using Ultrasoft Pseudopotentials. *Phys. Rev. B* **2007**, *76*, 024401.

(10) Monkhorst, H. J.; Pack, J. D. Special Points for Brillouin-Zone Integrations. *Phys. Rev. B* **1976**, *13*, 5188.